Int. J. Electrochem. Sci., 17 **(2022)** Article Number: 221265, doi: 10.20964/2022.12.78

International Journal of
ELECTROCHEMICAL
SCIENCE
www.electrochemsci.org

Preparation of CeO_2-coated $Li_{1.2}Mn_{0.54}Co_{0.13}Ni_{0.13}O_2$ as cathode materials for Lithium Ion Batteries

Jitie Sun[2,a], Zihao Zheng[2,a], Wenchao Xia[2], Lei Zhou[2], Yanan Wei[1,2], Fengli Bei [1,2,]*

[1] National Quality Supervision and Inspection Center for Industrial Explosive Materials, Nanjing University of Science and Technology, Nanjing 210094, P. R. China
[2] School of Chemistry and Chemical Engineering, Nanjing University of Science and Technology, Nanjing 210094, P. R. China
[*]E-mail: beifl@njust.edu.cn
[a] Jitie Sun and Zihao Zheng contributed equally to this work.

Received: 10 October 2022 / *Accepted:* 23 November 2022 / *Published:* 27 December 2022

Li-rich cathode material $Li_{1.2}Mn_{0.54}Co_{0.13}Ni_{0.13}O_2$ is an important candidate material for Li-ion batteries. However, due to its low initial coulombic efficiency, poor cycle performance and rate performance, its development has been limited. In order to stabilize the crystal structure and improve the electrochemical performance, CeO_2 was coated on the surface of $Li_{1.2}Mn_{0.54}Co_{0.13}Ni_{0.13}O_2$ by surface engineering strategy while doping trace amount of Ce. The results show that this modification method greatly reduced the Li/Ni mixing level in the material and mitigated the oxygen loss, which was beneficial to improve the electrochemical performance of the material. As expected, the initial cycle coulombic efficiency of the modified sample (4wt % - CeO_2) increased by 27.5% at 1 C, and the discharge capacity increased by 28.4% after 50 charge-discharge cycles at 0.2 C in the voltage range of 2.0 V to 4.8 V. In particular, the discharge specific capacity increased by 90.4% at a high rate of 10 C. This strongly proves that the strategy has great prospects in improving the electrochemical performance of Li-ion battery electrode materials.

Keywords: Li-rich cathode material; Li/Ni mixed; Oxygen loss; Surface engineering; High rate performance

1. INTRODUCTION

Nowadays, with the rapid progress of human society, traditional fossil fuels such as coal, oil and natural gas can no longer meet the needs of economic development. The ensuing energy depletion and environmental pollution have become the most serious challenges in the 21st century. Therefore, it is imperative to develop renewable energy [1-3]. Li-ion batteries have great advantages over all new energy sources in terms of energy conversion and storage [4, 5].

Li-ion batteries have been widely used in energy storage devices [6-11], portable electronics [12, 13] and some new energy vehicles [14-16], and have created huge economic value. As one of the key components of Li-ion batteries, cathode materials play a crucial role in determining the electrochemical performance and the cost of Li-ion batteries. Li-rich Mn-based cathode materials have many advantages, such as low toxicity, low cost and high discharge capacity of greater than 250 $mAh \cdot g^{-1}$ [17, 18]. It was first proposed by Thackeray and his colleagues in 1991 and has received extensive attention over the past decade [19]. However, due to the shortcomings such as low initial coulombic efficiency, rapid capacity loss and poor rate performance, Li-rich Mn-based cathode materials still need further improvement to meet the requirements of commercial applications [20-22].

These shortcomings of Li-rich cathode materials are closely related to lattice distortion and microstructure defects caused by oxygen release due to anion redox [23-26]. Moreover, the release of irreversible oxygen will further promote the Li/Ni mixing caused by the transition metals migrating to the lithium layer during the circulation process, thus accelerating the phase transition from the layer to spinel phase or even rock salt phase [27-29]. In addition, the direct contact between the electrolyte and the cathode material will produce side reactions during the charging and discharging process of the battery [1, 30], which will also lead to the degradation of the electrochemical performance.

To solve the above problems, people usually adopt the strategies such as morphology control [31-33], surface modification [34-38] and element doping [39-46]. Among them, surface modification is considered to be the most effective method to alleviate the phase transition caused by irreversible oxygen loss and side reactions in the electrolyte, while element doping can greatly inhibit the Li/Ni mixing. Previous studies have shown that Co doping can inhibit the Li/Ni mixing, but excessive Co increases the microcracks in the grains and exacerbates the structural collapse of the material [47, 48]. In addition, Al doping can also inhibit the Li/Ni mixing, but it may lead to the formation of new phase LiAlO2 and hinder the diffusion of Li ions [49]. Wu [50] investigated the effect of different coatings on the surface modification of Li-rich Mn-based cathode materials. It was found that Al2O3 and AlPO4 can effectively prevent the structural degradation by mitigating the oxygen loss.

In this paper, the effect of CeO_2 coating on the electrochemical performance of $Li_{1.2}Mn_{0.54}Co_{0.13}Ni_{0.13}O_2$ was investigated. After the original Li-rich material was prepared by co-precipitation-hydrothermal method, it was successfully coated and micro-doped by wet chemical deposition. It not only mitigates the irreversible oxygen loss, but also reduces the structural collapse caused by the mixing of lithium and nickel ions. At the same time, the side reaction between the cathode material and the electrolyte under high pressure is reduced, so that the first cycle performance and long-term cycle performance of the material are improved, and the charge and discharge performance at large rate is significantly improved.

2. EXPERIMENTAL

2.1 Preparation of cathode

The original cathode material was prepared by co-precipitation-hydrothermal method. Unlike Pechini methods, $NiSO_4 \cdot 6H_2O$, $CoSO_4 \cdot 7H_2O$ and $MnSO_4 \cdot H_2O$ (molar ratio of 4:1:1) were used instead of $Ni(NO_3)_2 \cdot 6H_2O$, $Co(NO_3)_2 \cdot 6H_2O$ and $Mn(NO_3)_2 \cdot 4H_2O$ as raw materials [51]. Deionized

water was added to prepare 2 mol·L^{-1} solution. In a nitrogen atmosphere, the precipitant NaOH and the complexing agent $NH_3 \cdot H_2O$ was slowly added dropwise with the concentrations of 4 mol·L^{-1} and 2 mol·L^{-1}, respectively. The pH of the solution was adjusted to 11 with dilute hydrochloric acid. After stirring in nitrogen atmosphere for 2 h, it was transferred to a hydrothermal kettle and reacted at 200 °C for 12 h. After the reaction, the resulting precipitate was washed three times with deionized water and alcohol,respectively, and dried overnight in a drying oven. Li_2CO_3 was used as a lithium source to fully mix and grind with the above-mentioned precursor (molar ratio of 1:1.26). The mixture was transferred into a tube furnace, pre-sintered at 450 °C for 5 h in an oxygen atmosphere, and then calcined at 850 °C for 15 h. The original cathode material $Li_{1.2}Mn_{0.54}Co_{0.13}Ni_{0.13}O_2$ (labeled as pristine) was obtained after natural cooling at room temperature.

2.2 Preparation of modified cathode materials

The original material was coated with CeO_2 by wet chemical deposition method. The specific synthesis method is as follows: A certain amount of original material $Li_{1.2}Mn_{0.54}Co_{0.13}Ni_{0.13}O_2$ powder was put into deionized water and ultrasonically dispersed for 20 min. Then, 2 mol·L-1 $Ce(NO_3)_3 \cdot 6H_2O$ solution was slowly dripped into the above solution under continuous stirring. After dripping, the solution was placed in a 75 °C water bath, and the stirring continued until the water evaporated and dried. The CeO_2-coated $Li_{1.2}Mn_{0.54}Co_{0.13}Ni_{0.13}O_2$ material was obtained by calcining the obtained powder in a tube furnace at 450 °C for 4 h in an oxygen atmosphere. The addition amount of CeO_2 was controlled by adjusting the mass ratio of $Ce(NO_3)_3 \cdot 6H_2O$ to the original material. The mass ratio of CeO_2 addition to the original material was 1 wt%, 2 wt% and 4 wt%, which was respectively labeled as 1 wt%-CeO_2, 2 wt%- CeO_2 and 4 wt%- CeO_2.

2.3 Material characterization

The material was tested by D8 advance X-ray diffractometer (XRD) produced by German Bruker Company to analyze its crystal structure. The test tube voltage was 40 kV, and the tube current was 40 mA. The Cu-Kα radiation source with a wavelength of 0.15406 nm and the graphite monochromator were used. The scanning speed was 10 °/min with a step size was 0.05 ° in a 2θ scanning range of 10 ° ~ 80 °. The thickness, particle shape and size of the material with different resolutions were observed using a JEM-1400 plus transmission electron microscope (TME) produced by Japan Electronics. A scanning electron microscope (SEM) of Quanta FEG 250 made in the United States was used to observe the surface morphology of the material. The oxidation state of a metal element in the sample was determined by X-ray photoelectron spectroscopy (XPS) analysis, using the AXIS-UITRADLD model produced by Kratos, a British company.

2.4 Electrochemical performance test

The CR2016 button cell used in this experiment was assembled in a glove box filled with argon. The anode was a high-purity lithium sheet, the separator was a porous polypropylene membrane Celgard

2400, and the electrolyte was 1 mol/L $LiPF_6$/(EC+DEC+EMC). The volume ratio of EC (ethylene carbonate), DEC (diethyl carbonate) and EMC (methyl ethyl carbonate) was 1:1:1. The positive electrode was made of positive active material, polyvinylidene fluoride (PVDF) and acetylene black and N-methyl pyrrolidone (NMP) in a mass ratio of 8:1:1 on aluminum foil. The assembly was carried out according to the sequence of negative shell, lithium sheet, diaphragm, electrolyte, positive electrode sheet, gasket, spring and positive shell. The sealing pressure of the sealing machine was 50 MPa. The charging and discharging test of the above batteries was carried out by using the button 3000-1 type blue electric test system produced by Wuhan Lambo Test Equipment Co., Ltd. The voltage range is 2.0 V ~ 4.8 V, and the test content is: 50 cycles of charge and discharge at 0.2 C rate. The rate performance was tested at current densities of 0.1 C, 0.2 C, 0.5 C, 1 C, 2 C, 5 C and 10 C, where 1 C = 200 $mAh \cdot g^{-1}$. The CHI660 C electrochemical workstation produced by Shanghai Chenhua Instrument Company was used to perform cyclic voltammetry test and AC impedance test on the battery. The cyclic voltammetry test started from the open-circuit voltage of the battery, with the scanning rate of 0.1 $mV \cdot S^{-1}$ and the voltage range of 2.0 V ~ 4.8 V. The test potential for the AC impedance test was 5 mV, and the frequency range was 0.01 to 100,000 Hz.

3. RESULTS AND DISCUSSION

3.1 Morphological characteristics of the material

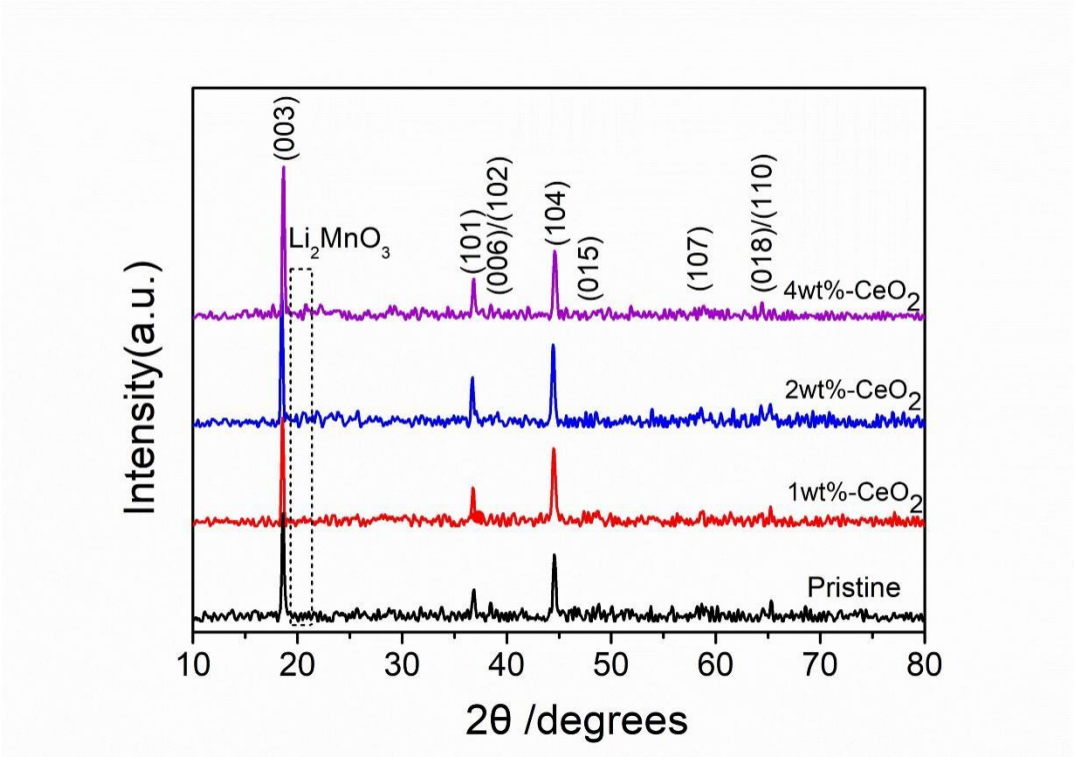

Figure 1. XRD patterns of 1wt % - CeO_2, 2wt % - CeO_2, 4wt % - CeO_2 and the Pristine samples (scanning speed of 10 °/min, the scanning range of 2θ = 10 ° - 80 ° and step size of 0.05 °).

Figure 1 shows the XRD patterns of the samples with different CeO_2 additions. It can be seen from the Fig. 1 that the diffraction peaks of the synthesized materials before and after modification correspond to the layered structure of the α-$NaFeO_2$ type with the space group of R3m [52]. The weak peaks between 20 ° and 25 ° is attributed to the Li_2MnO_3 phase with the space group of C2/m, which belongs to the characteristic peak of the Li-rich material [53]. The peak splitting of the (018)/(110) crystal plane of the four samples is clear, indicating that the layered structure of the material before and after modification has good crystallinity. The value of I(003)/I(104) indicates the Li/Ni mixing level. The higher the value, the lower the Li/Ni mixing level [54-57]. It can be clearly seen that with the increase of the addition amount, the ratio of diffraction peak intensity of (003) to (104) crystal plane increases significantly, indicating that CeO_2 coating and trace Ce doping can effectively inhibit Li/ Ni mixing.

Table 1. Crystal parameters of 1wt % - CeO_2 and the Pristine samples refined by Jade software.

Sample	a/Å	c/Å	c/a
Pristine	2.83781	14.32603	5.04872
1wt%- CeO_2	2.83393	14.33862	5.05962

Table 1. is the crystal parameters of the Pristine and 1 wt%-CeO_2 samples refined by Jade software. It can be seen from the table that the changes of cell parameters is caused by the diffusion of trace cerium ions into the crystal during the high-temperature sintering, and the successful doping of cerium ions into the transition metal layer of the material, thus changing the crystal structure.

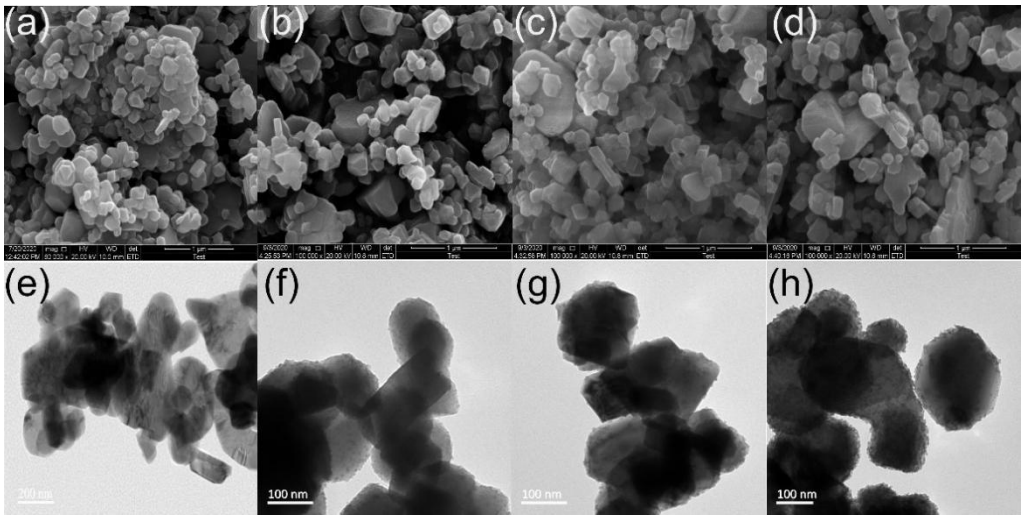

Figure 2.SEM images of (a) Pristine, (b) 1wt%- CeO_2, (c) 2wt%- CeO_2, (d) 4wt% CeO_2 samples and TEM images of (e) Pristine, (f) 1wt%- CeO_2, (g) 2wt%- CeO_2, (h) 4wt%- CeO_2 samples

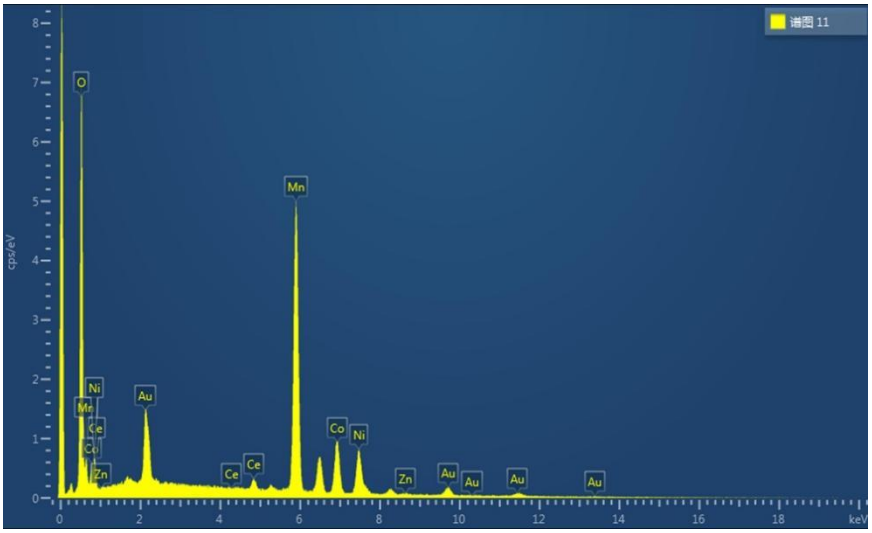

Figure 3. EDS spectrum of 2wt % - CeO_2 sample

The SEM and TEM images of 1 wt%-CeO_2, 2 wt%- CeO_2, 4 wt%- CeO_2 and the Pristine are shown in **Figure 2.** It can be seen from the SEM images that the morphology and particle size of the material have not changed significantly before and after modification. The average particle size is 200 ~ 300 nm with good dispersion. The surface of the original material particles is smooth, and the interface between the three modified sample particles is gradually blurred, which is because CeO_2 nanoparticles are coated on the surface of the material. It can be observed from the TEM images that the coating composed of CeO_2 nanoparticles is not uniform when the addition amount is 1 wt% and 2 wt%, which may be due to the small amount of coating and may not have a good protective effect on the active material. When the addition amount is 4 wt%, a dense and uniform coating with a thickness of about 2 nm appears on the surface of the particles. The dense and uniform coating can reduce and delay the destruction of the layered structure of the material, which is beneficial to improving the electrochemical performance of the material.

Figure 3 is the EDS spectrum of 2 wt%-CeO_2 sample, which proves that CeO_2 is indeed coated on the surface of the original material.

3.2 Electrochemical performance of materials

Figure 4 is the first charge-discharge specific capacity diagram of 1 wt%-CeO_2, 2 wt%- CeO_2, 4 wt%- CeO_2 and the Pristine samples. It can be seen from **Figure 4** that the first charging curve of the material before and after modification consists of two obvious charging platforms, which is the typical first charging curve of a Li-rich layered oxide. The initial discharge specific capacities of the original material and the samples with the addition of 1 wt%, 2 wt% and 4 wt% were 264.0 $mAh \cdot g^{-1}$, 307.4 $mAh \cdot g^{-1}$, 321.0 $mAh \cdot g^{-1}$ and 346.5 $mAh \cdot g^{-1}$, respectively. The corresponding coulombic efficiencies were 58.38 %, 67.10 %, 71.98 % and 74.45 %, respectively. This was higher than the initial discharge specific capacity of 261.81 $mAh \cdot g^{-1}$ and the corresponding coulombic efficiency of 69.1% of

$Li_{1.2}Mn_{0.54}Co_{0.13}Ni_{0.13}O_2$ coated with CeO_2 by traditional hydrothermal method [58]. It can also be seen that the discharge specific capacity of the modified samples is improved, and the first cycle coulombic efficiency is gradually improved with the increase of the addition amount. This is because some oxygen vacancies remain in the crystal lattice after CeO_2 coating, which inhibits the irreversible oxygen loss, thereby effectively reducing the loss of the first irreversible capacity and improving the discharge specific capacity of the modified material.

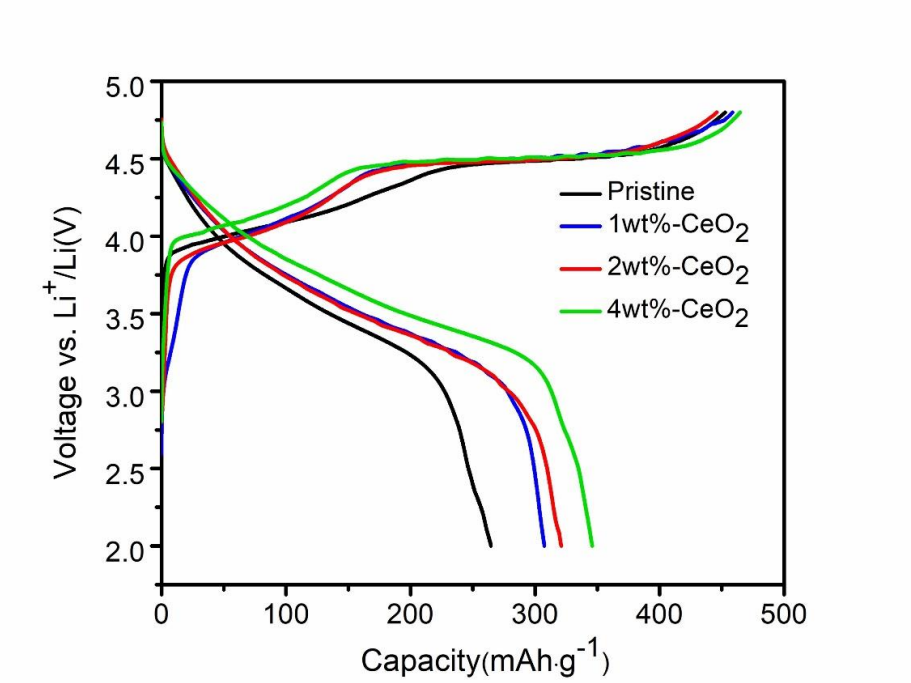

Figure 4. The initial charge-discharge curve of 1 wt%-CeO_2, 2 wt%-CeO_2, 4 wt%-CeO_2 and the Pristine samples (at 0.1 C, voltage range of 2.0 V ~ 4.8 V).

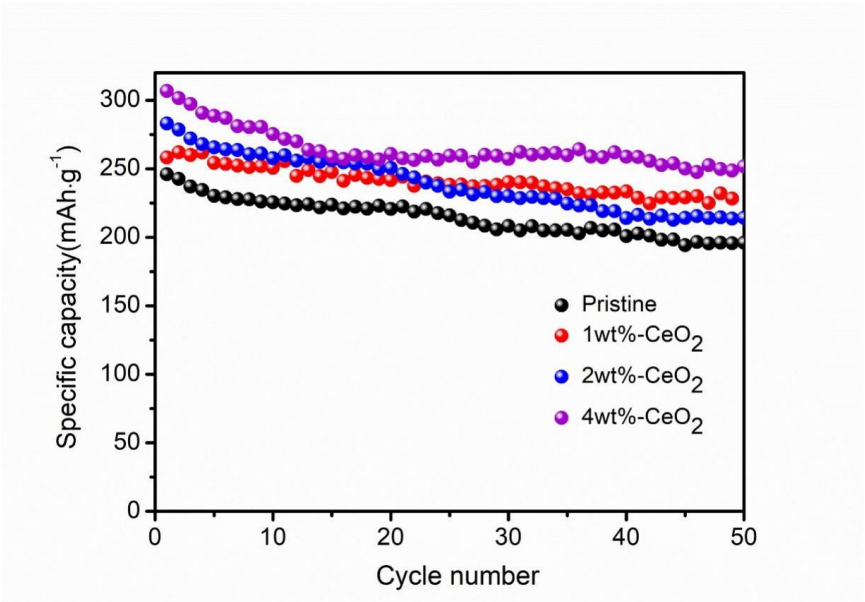

Figure 5. Cycle performance of 1 wt%-CeO_2, 2 wt%-CeO_2, 4 wt%-CeO_2 and the Pristine samples (at 0.2 C, voltage range of 2.0 V ~ 4.8 V).

Figure 5 is the cycle performance diagram of 1 wt%-CeO_2, 2 wt%-CeO_2, 4 wt%-CeO_2 and the Pristine samples under the conditoins of 0.2 C, voltage range of 2.0 V ~ 4.8 V and 50 cycles of charge and discharge. As can be seen from the **Figure 5**, after 50 charge and discharge cycles, the discharge specific capacity of the original material and the sample with the addition amount of 1 wt%, 2 wt% and 4 wt% were 196.0 mAh·g^{-1}, 228.3 mAh·g^{-1}, 214.2 mAh·g^{-1} and 251.7 mAh·g^{-1}, respectively. It can be seen that with the increase of the addition amount, the discharge specific capacity of the material gradually increases after 50 cycles. This is because in the unmodified sample, Ni^{2+} ions in the transition metal layer will mix with Li^+ ions with the occurrence of redox reaction. After multiple charge-discharge cycles, the material changes from a layered structure to a spinel structure, which hinders the transmission of lithium ions. After modification, cerium ions replace part of the transition metal ions, which reduces the mixing level of lithium and nickel, and the material structure is stable, so the cycle performance is better. It can be seen that the specific capacity of the sample with 4 wt% addition is higher than that of the samples with 1 wt% and 2 wt% addition. This is because the relatively high addition amount forming a relatively uniform cerium oxide coating, which can effectively inhibit the interface reaction between the material and the electrolyte, reduce the serious corrosion of acidic substances to the electrode material and reduce the degradation of the material structure [59-61].

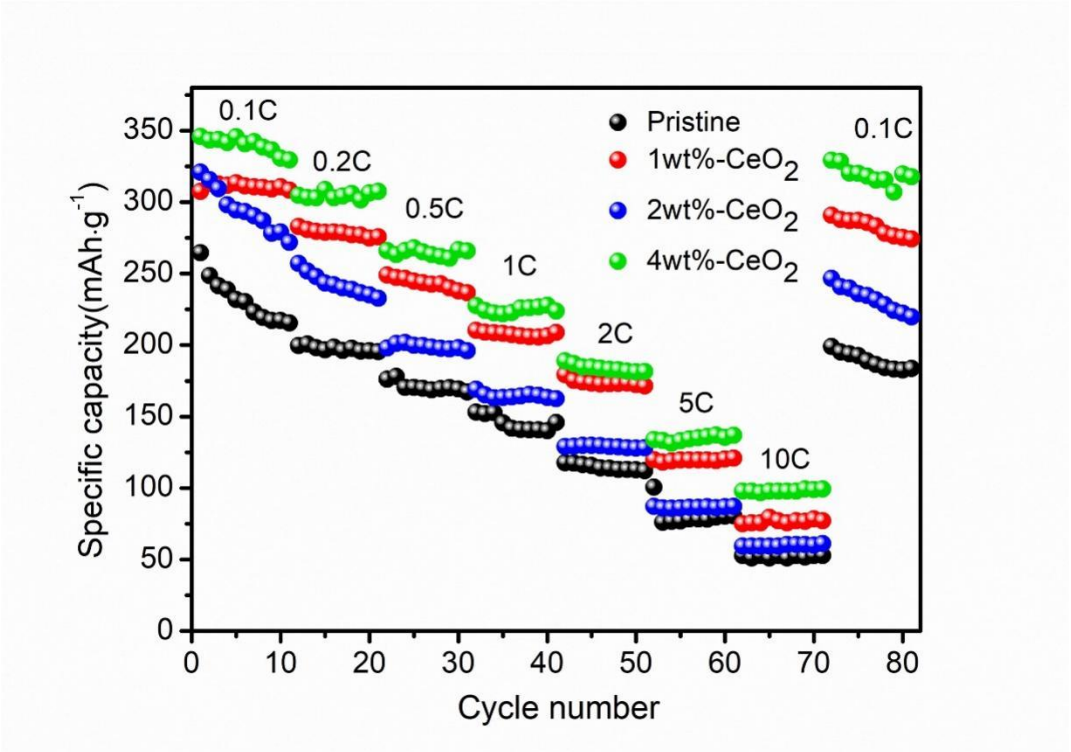

Figure 6. Rate performance of 1 wt%-CeO_2, 2 wt%-CeO_2, 4 wt%-CeO_2 and the Pristine samples (voltage range of 2.0 V ~ 4.8 V).

Figure 6 is the rate performance of 1 wt%-CeO_2, 2 wt%-CeO_2, 4 wt%-CeO_2 and the Pristine samples. The test voltage range is 2.0 V ~ 4.8 V. It can be seen from **Figure 6** that the discharge specific capacities of the original material and the samples with the addition amount of 1 wt%, 2wt % and 4wt % at high rate of 10 C are 52.3 mAh·g^{-1},77.5mAh·g^{-1},60.3mAh·g^{-1} and 99.6mAh·g^{-1}, respectively. The discharge specific capacity of the modified material at high rate of 10 C is significantly improved,

especially the 4 wt%-CeO_2 sample, showing the rate performance of the pole. On the one hand, the surface of the material has a dense, uniform and stable coating layer, which reduces the irreversible oxygen loss. On the other hand, doping inhibits the cation mixing. The combination of the two stabilizes the layered structure of the material and inhibits the transformation of the layered structure to spinel or even rock salt phase structure, making it easier for lithium ions to embed and detach, thereby improving the rate performance of the material.

Table 2. Rate performance of $Li_{1.2}Mn_{0.54}Co_{0.13}Ni_{0.13}O_2$ cathode materials modified by different coatings. (* Here is the "4 wt%-CeO_2" in this article)

Coatings	0.1 C $mAh \cdot g^{-1}$	0.2 C $mAh \cdot g^{-1}$	0.5 C $mAh \cdot g^{-1}$	1 C $mAh \cdot g^{-1}$	2 C $mAh \cdot g^{-1}$	5 C $mAh \cdot g^{-1}$	10 C $mAh \cdot g^{-1}$	Ref.
Bi_2O_3	250	225	175	150	125	90	/	[62]
Co_3O_4	270	230	185	150	125	98	/	[63]
TiO_2	275	240	200	175	145	75	/	[64]
MoO_3	275	240	210	175	150	110	/	[65]
V_2O_5	280	/	/	185	170	115	75	[66]
CeO_2	330	305	270	225	180	125	100	*

Table 2 shows the rate performance of $Li_{1.2}Mn_{0.54}Co_{0.13}Ni_{0.13}O_2$ cathode materials modified by different coatings. It can be seen intuitively from **Table 2** that CeO_2, as a coating material, has a significant advantage in improving the rate performance of $Li_{1.2}Mn_{0.54}Co_{0.13}Ni_{0.13}O_2$ cathode materials.

Figure 7 is the cyclic voltammetry curves of 1wt % - CeO_2,2wt % - CeO_2,4wt % - CeO_2 and the Pristine samples in the first three cycles of charge and discharge. It can be seen from the **Figure 7** that the curves of the four samples are consistent with the typical cyclic voltammetry curves of Li-rich Mn-based cathode materials. In the first cyclic voltammetry curve, there are two obvious anode peaks, corresponding to the two platforms in the first charging curve. The first anode peak is located at about 4.0 V, which corresponds to the extraction of lithium ions in the $LiMO_2$ structure, that is, $LiMO_2 \rightarrow MO_2 + Li^+ + e$-, accompanied by the oxidation of Ni^{2+} to Ni^{4+} and Co^{3+} to Co^{4+}; the second anode peak is located at about 4.5 V, which corresponds to the activation of Li2MnO3 to form electrochemically active MnO_2. The corresponding reaction is $Li_2MnO_3 \rightarrow MnO_2 + 2Li^+ + 1/2O^{2+}\ 2e^-$[67]. As the deintercalation of Li_2O is irreversible, the second anode peak will disappear in the next cycle. In addition, the cycle curves of the second and third cycles can overlap each other well, which indicates that all the

other processes are reversible except the irreversible activation of Li_2MnO_3 in the first cycle, and the coincidence degree of the modified sample is better than that of the original material. It shows that the cerium oxide coating in surface engineering can stabilize the structure of the material and improve the reversibility of the material.

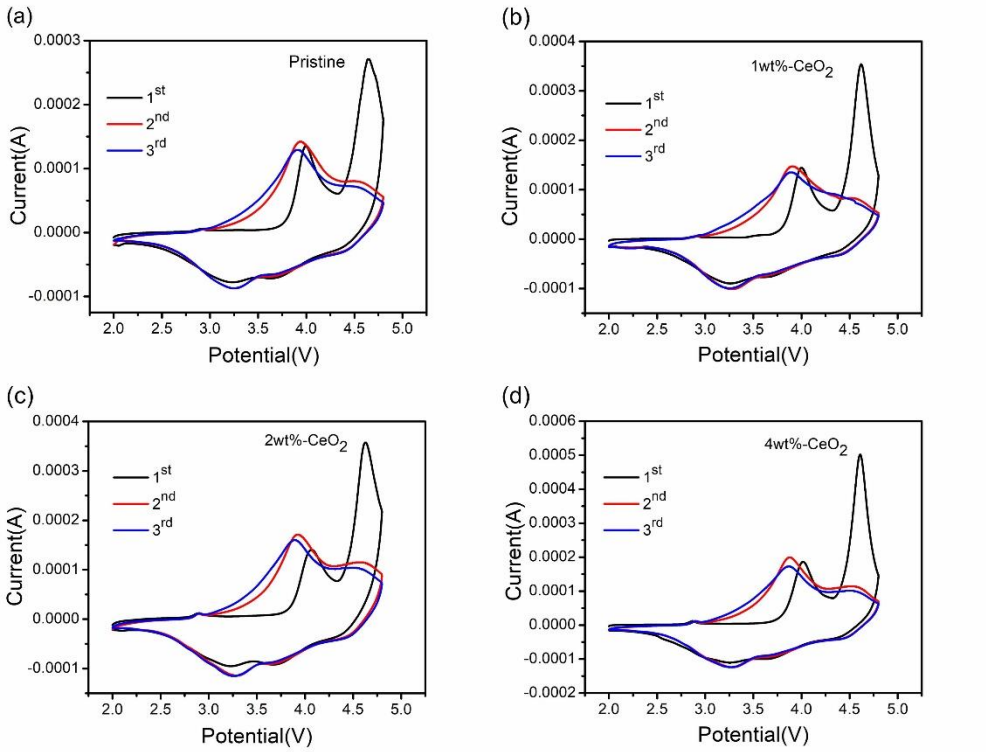

Figure 7. CV curves of (a) Pristine, (b) 1 wt%-CeO_2, (c) 2 wt%-CeO_2 and (d) 4 wt%-CeO_2 samples (scanning rate of 0.1 mV·s-1, voltage range of 2.0 V ~ 4.8 V).

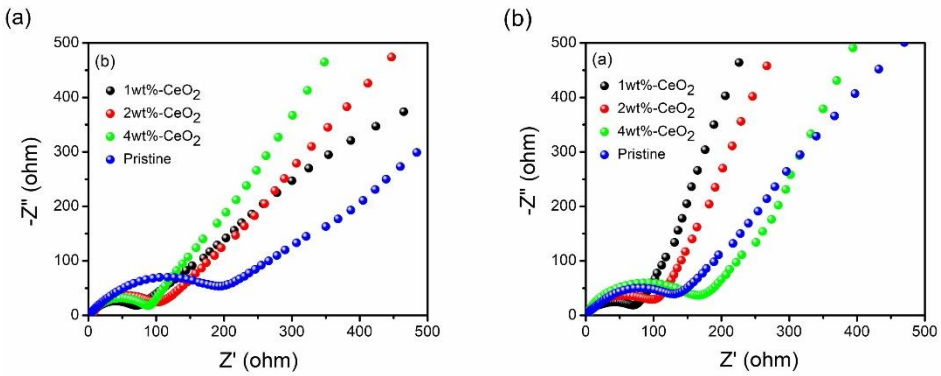

Figure 8. Nyquist plots of samples (a) in the first cycle and (b) after 50 cycles (potential of 5 mV, frequency range of 0.01~100,000 Hz).

Figure 8 is the AC impedance diagram of 1wt % - CeO_2,2wt % - CeO_2,4wt % - CeO_2 and the Pristine samples tested in the first cycle and after 50 cycles. Re and Rct represent solution resistance and

charge transfer resistance, respectively. It can be seen that after modification, the Rct value is reduced after 50 cycles. The smaller Rct value means that the diffusion of Li^+ ions is increased due to the improvement of interface properties.

4. CONCLUSIONS

In summary, we report a green surface engineering strategy for Li-rich cathode materials for Li-ion batteries. The carbonate precursor of the Li-rich material was synthesized by co-precipitation-hydrothermal method, and then uniformly mixed with lithium carbonate to form the Li-rich material. CeO_2 coating was applied to the surface of the material by wet chemical deposition. Ce diffused into the crystal lattice to replace the metal ions and increased the internal defects of the material. Under the synergistic effect of coating and doping, the electrochemical performance of Li-rich materials has been improved as a whole, and the charge and discharge performance at high rates has been significantly improved. This surface engineering strategy also has a profound impact on improving the cycling and storage performance of other Li-ion battery cathode materials.

ACKNOWLEDGEMENTS
The work is supported by the National Natural Science Foundation of China (No. 51472119 and 21474053).

References

1. E. Hu, X. Yu, R. Lin, X. Bi, J. Lu, S. Bak, K.-W. Nam, H. L. Xin, C. Jaye, D. A. Fischer, K. Amine, X.-Q. Yang, *Nat. Energy*, 3(2018)690.
2. G. Wang, X. Xiong, D. Xie, Z. Lin, J. Zheng, F. Zheng, Y. Li, Y. Liu, C. Yang, M. Liu, *J. Mater. Chem. A*, 6(2018)24317.
3. K. Wu, D. Liu, Y. Tang, *Electrochim. Acta*, 263(2018)515.
4. L.-L. Zhang, Z. Li, X.-L. Yang, X.-K. Ding, Y.-X. Zhou, H.-B. Sun, H.-C. Tao, L.-Y. Xiong, Y.-H. Huang, *Nano Energy*, 34(2017)111.
5. Z. Qiu, Y. Zhang, X. Huang, J. Duan, D. Wang, G. P. Nayaka, X. Li, P. Dong, *J. Power Sources*, 400(2018)341.
6. S.-T. Myung, F. Maglia, K.-J. Park, C. S. Yoon, P. Lamp, S.-J. Kim, Y.-K. Sun, *ACS Energy Lett.*, 2(2017)196.
7. D. Larcher, J. M. Tarascon, *Nat. Chem.*, 7(2015)19.
8. M. S. Whittingham, *Chem. Rev.*, 114(2014)11414.
9. F. Sun, X. Hu, Y. Zou, S. Li, *Energy*, 36(2011)3531.
10. S. B. Peterson, J. Apt, J. F. Whitacre, *J. Power Sources*, 195(2010)2385.
11. M. Armand, J. M. Tarascon, *Nature*, 451(2008)652.
12. A. Ritchie, W. Howard, *J. Power Sources*, 162(2006)809.
13. B. Scrosati, *Chem. Rec.*, 5(2005)286.
14. L. Lu, X. Han, J. Li, J. Hua, M. Ouyang, *J. Power Sources*, 226(2013)272.
15. X. Zeng, M. Li, D. Abd El-Hady, W. Alshitari, A. S. Al-Bogami, J. Lu, K. Amine, *Adv. Energy Mater.*, 9(2019) 1900161.
16. S. T. Myung, F. Maglia, K. J. Park, S. Y. Chong, Y. K. Sun, *ACS Energy Lett.*, 2(2016)196.
17. J. Rana, M. Stan, R. Kloepsch, J. Li, G. Schumacher, E. Welter, I. Zizak, J. Banhart, M. Winter,

Adv. *Energy Mater.*, 4(2014) 1300998.
18. N. Yabuuchi, M. Takeuchi, M. Nakayama, H. Shiiba, M. Ogawa, K. Nakayama, T. Ohta, D. Endo, T. Ozaki, T. Inamasu, K. Sato, S. Komaba, *Proc. Natl. Acad. Sci. U.S.A.*, 112(2015)7650.
19. MH, Rossouw, and, MM, Thackeray, *Mater. Res. Bull.*, 26(1991)463.
20. X. Ji, Q. Xia, Y. Xu, H. Feng, Q. Tan, *J. Power Sources*, 487(2021)229362.
21. S. Li, H. Li, H. Zhang, S. Zhang, Y. Lai, Z. Zhang, *Chem. Eng. J.*, 427(2022) 229362.
22. A. Boulineau, L. C. Simonin, J. F. O. Colin, C. Bourbon, S. Patoux, *Nano Lett.*, 13(2013)3857.
23. W. Li, H. Y. Asl, Q. Xie, A. Manthiram, *J. Am. Chem. Soc.*, 141(2019)5097.
24. A. O. Kondrakov, A. Schmidt, J. Xu, H. Gesswein, R. Moenig, P. Hartmann, H. Sommer, T. Brezesinski, J. Janek, *J. Phys. Chem. C*, 121(2017)3286.
25. L. Wang, Y. G. Sun, L. L. Hu, J. Y. Piao, J. Guo, A. Manthiram, J. M. Ma, A. M. Cao, *J. Mater. Chem. A*, 5(2017)8752
26. J. Li, R. Shunmugasundaram, R. Doig, J. R. Dahn, *Chem. Mater.*, 28(2016)162.
27. F. Fu, Y.-P. Deng, C.-H. Shen, G.-L. Xu, X.-X. Peng, Q. Wang, Y.-F. Xu, J.-C. Fang, L. Huang, S.-G. Sun, *Electrochem. Commun.*, 44(2014)54.
28. M. Oishi, K. Yamanaka, I. Watanabe, K. Shimoda, T. Matsunaga, H. Arai, Y. Ukyo, Y. Uchimoto, Z. Ogumi, T. Ohta, *J. Mater. Chem. A*, 4(2016)9293.
29. F. Zheng, C. Yang, X. Xiong, J. Xiong, R. Hu, Y. Chen, M. Liu, *Angew. Chem. Int. Ed.*, 54(2015)13058.
30. Z. Xue, X. Qi, L. Li, W. Li, L. Xu, Y. Xie, X. Lai, G. Hu, Z. Peng, Y. Cao, K. Du, *ACS Appl. Mater. Interfaces*, 10(2018)27141.
31. J. Fang, H. An, F. Qin, H. Wang, C. Chen, X. Wang, Y. Li, B. Hong, J. Li, *ACS Appl. Mater. Interfaces*, 12(2020)55926.
32. Y. Ma, P. Liu, Q. Xie, G. Zhang, H. Zheng, Y. Cai, Z. Li, L. Wang, Z.-Z. Zhu, L. Mai, D.-L. Peng, *Nano Energy*, 59(2019)184.
33. D.-S. Ko, J.-H. Park, S. Park, Y. N. Ham, S. J. Ahn, J.-H. Park, H. N. Han, E. Lee, W. S. Jeon, C. Jung, *Nano Energy*, 56(2019)434.
34. B. Niu, J. Li, Y. Liu, Z. Li, Z. Yang, *Ceram. Int.*, 45(2019)12484.
35. A. Panda, J. Patra, C.-T. Hsieh, Y.-C. Huang, Y. A. Gandomi, C.-C. Fu, M.-H. Lin, R.-S. Juang, J.-K. Chang, *J. Energy Storage*, 44(2021) 103348.
36. Z. He, J. Li, Z. Luo, Z. Zhou, X. Jiang, J. Zheng, Y. Li, J. Mao, K. Dai, C. Yan, Z. Sun, *ACS Appl. Mater. Interfaces*, 13(2021)49390.
37. L. Xu, Z. Sun, Y. Zhu, Y. Han, M. Wu, Y. Ma, Y. Huang, H. Zhang, Y. Chen, *Sci. China Mater.*, 63(2020)2435.
38. Z. Xu, L. Ci, Y. Yuan, X. Nie, J. Li, J. Cheng, Q. Sun, Y. Zhang, G. Han, G. Min, J. Lu, *Nano Energy*, 75(2020) 104942.
39. Y. Tang, X. Han, W. Zhang, Y. He, *Ionics*, 26(2020)3737.
40. H. Chen, W. Li, *Ionics*, 28 (2022)2083.
41. C. Zhang, B. Wei, W. Jiang, M. Wang, W. Hu, C. Liang, T. Wang, L. Chen, R. Zhang, P. Wang, W. Wei, *ACS Appl. Mater. Interfaces*, 13(2021)45619.
42. L. Nie, Z. Wang, X. Zhao, S. Chen, Y. He, H. Zhao, T. Gao, Y. Zhang, L. Dong, F. Kim, Y. Yu, W. Liu, *Nano Lett.*, 21(2021)8370.
43. Y.-H. Liu, T.-Y. Tsai, *J. Power Sources*, 484(2021) 229262.
44. G. Liang, V. K. Peterson, Z. Wu, S. Zhang, J. Hao, C.-Z. Lu, C.-H. Chuang, J.-F. Lee, J. Liu, G. Leniec, S. M. Kaczmarek, A. M. D'Angelo, B. Johannessen, L. Thomsen, W. K. Pang, Z. Guo, *Adv. Mater.*, 33(2021) 2101413.
45. J. Zhong, Z. Yang, Y. Yu, Y. Liu, J. Li, F. Kang, *Appl. Surf. Sci.*, 512(2020) 145741.
46. P. Zhang, X. Zhai, H. Huang, J. Zhou, X. Li, Y. He, Z. Guo, *Electrochim. Acta*, 349(2020) 136402.
47. T. Liu, L. Yu, J. Liu, J. Lu, X. Bi, A. Dai, M. Li, M. Li, Z. Hu, L. Ma, D. Luo, J. Zheng, T. Wu, Y. Ren, J. Wen, F. Pan, K. Amine, *Nat. Energy*, 6(2021)277.

48. E. Boivin, N. Guerrini, R. A. House, J. G. Lozano, L. Jin, G. J. Rees, J. W. Somerville, C. Kuss, M. R. Roberts, P. G. Bruce, *Adv. Funct. Mater.*, 31(2021) 2003660.
49. B. Pei, H. Zhou, A. Goel, M. Zuba, H. Liu, F. Xin, M. S. Whittingham, *J. Electrochem. Soc*, 168(2021)1.
50. Y. Wu, A. Manthiram, *Solid State Ionics*, 180(2009)50.
51. C. Wu, X. Fang, X. Guo, Y. Mao, J. Ma, C. Zhao, Z. Wang, L. Chen, *J. Power Sources*, 231(2013)44.
52. G. Arnold, J. Garche, R. Hemmer, S. Strobele, C. Vogler, A. Wohlfahrt-Mehrens, *J. Power Sources*, 119(2003)247.
53. W. Wang, G. Hu, Z. Peng, K. Du, Y. Cao, J. Duan, *Ceram. Int.*, 44(2018)1425.
54. G. Hu, M. Zhang, L. Wu, Z. Peng, K. Du, Y. Cao, *ACS Appl. Mater. Interfaces*, 8(2016)33546.
55. W. Lee, S. Muhammad, T. Kim, H. Kim, E. Lee, M. Jeong, S. Son, J.-H. Ryou, W.-S. Yoon, *Adv. Energy Mater.*, 8(2018) 1870015.
56. N. D. Rago, J. Bareno, J. Li, Z. Du, D. L. Wood, III, L. A. Steele, J. Lamb, S. Spangler, C. Grosso, K. Fenton, I. Bloom, *J. Power Sources*, 385(2018)148.
57. H. Xie, K. Du, G. Hu, Z. Peng, Y. Cao, *J. Phys. Chem. C*, 120(2016)3235.
58. L. J. Zhou, Z. L. Yin, Z. Y. Ding, X. H. Li, H. J. Guo, *Ionics*, 24(2017)1.
59. Y. Xu, X. Li, Z. Wang, H. Guo, W. Peng, W. Pan, *Electrochim. Acta*, 219(2016)49.
60. G. Yan, R. L. Patel, K. Y. Shen, X. Wang, X. Liang, *ACS Omega*, 3(2018)906.
61. S. Dong, Y. Zhou, C. Hai, J. Zeng, L. Ma, *Ceram. Int.*, 45(2018)144.
62. Z. Lin, H. Wu, M. Tian, Q. Zheng, C. Xu, D. Lin, *RSC Adv.*, 6(2016)69790.
63. L. Yu, H. Hui, J. Yu, X. Yang, C. Liang, Y. Gan, J. Zhang, W. Zhang, *J. Alloys Compd.*, 783(2019)349.
64. C. Song, W. Feng, Z. Shi, Z. Huang, *Ionics*, 27(2021)457.
65. C. Wang, F. Zhou, K. Chen, J. Kong, Y. Jiang, G. Yan, J. Li, C. Yu, W. P. Tang, *Electrochim. Acta*, 176(2015)1171.
66. H. He, L. Zan, Y. Zhang, *J. Alloys Compd.*, 680(2016)95.
67. K. Mu, Y. Cao, G. Hu, K. Du, H. Yang, Z. Gan, Z. Peng, *Electrochim. Acta*, 273(2018)88.